JCTC Journal of Chemical Theory and Computation

A General Boundary Potential for Hybrid QM/MM Simulations of Solvated Biomolecular Systems

Tobias Benighaus and Walter Thiel*

Max-Planck-Institut für Kohlenforschung, Kaiser-Wilhelm-Platz 1 45470, Mülheim an der Ruhr, Germany

Abstract: We present a general boundary potential for the efficient and accurate evaluation of electrostatic interactions in hybrid quantum mechanical/molecular mechanical (QM/MM) approaches called solvated macromolecule boundary potential (SMBP), which is designed for QM/MM calculations with any kind of QM method. The SMBP targets QM/MM single-point energy calculations and geometry optimizations. In the SMBP scheme, the outer solvent and macromolecule region is described by a boundary potential obtained with the use of Poisson−Boltzmann calculations (treating the bulk solvent as a dielectric continuum). In the QM calculations, the SMBP is represented by virtual point charges on a surface enclosing the explicitly treated inner region. These charges and their interactions with the QM density are determined through a self-consistent reaction field procedure. The accuracy of the SMBP is evaluated on three diverse test systems: the intramolecular proton transfer of glycine in water, the hydroxylation reaction in *p*-hydroxybenzoate hydroxylase, and the spin state energy splittings in the pentacoordinated ferric complex of cytochrome P450cam. In the case of solvated glycine, application of the SMBP turns out to be problematic since analogous QM/MM/SMBP and full QM/MM geometry optimizations lead to different close-lying local minima. In both enzymes, the SMBP performs very well and closely reproduces the results from full QM/MM optimizations of these more rigid test systems. Starting from optimized QM/MM/SMBP structures along a reaction path, one can apply the previously implemented generalized solvent boundary potential (GSBP) to sample over MM phase space in QM/MM free energy calculations within the framework of free energy perturbation theory. This reduces the overall computational costs of sampling by 1 order of magnitude while maintaining good accuracy. The combined use of SMBP and GSBP thus allows for efficient QM/MM free energy studies of enzymes.

1. Introduction

Hybrid quantum mechanical/molecular mechanical (QM/MM) methods have become established tools for studying large biomolecules, with an increasing number of applications being devoted to the computation of free energy differences.[1−12] In these systems, long-range electrostatic interactions can have a significant influence on the stability of transition states or the relative energies of different configurations. Therefore, an accurate description of these interactions is indispensable for meaningful computations of properties that require extensive

configurational sampling, for example, free activation or reaction energies.[13−16] While the development of efficient and accurate methods to describe electrostatic interactions improved the reliability of classical molecular dynamics (MD) simulations significantly,[14] these methods have only recently been adapted to the QM/MM framework.[17−21]

In the context of biomolecular simulations, one is frequently interested in localized processes in small active regions. The surrounding outer region often only serves to exclude solvent molecules, to constrain the active site geometries, and to provide a suitable electrostatic potential that supports a catalytic reaction, for example, by stabilization

---

* Corresponding author e-mail: thiel@mpi-muelheim.mpg.de.

of the transition state. For this class of systems, boundary potentials are suitable for treating long-range electrostatic interactions.[22−33] In this approach, the biomolecular system is subdivided into an inner region, comprising the active site and the adjacent part of the enzyme, and an outer region, comprising the rest of the enzyme and the outer solvent molecules. A perfect boundary potential describes the entire effect of the outer region such that the statistical properties of the inner region interacting with the boundary potential are identical to those of the full solvated biomolecule. Consequently, the boundary potential may be constructed rigorously by integration over all degrees of freedom of the outer region.[33] An efficient implementation, however, necessitates the introduction of further approximations.

The generalized solvent boundary potential (GSBP) developed by Im et al. in 2001 is a notably attractive and successful boundary potential.[34] In this approach, the outer region solvent molecules are represented by a polarizable dielectric continuum (PDC) and the outer region charge distribution by fixed point charges. Electrostatic interactions with the outer region are separated into a static solvent-shielded field induced by the outer region point charges interacting with the dielectric, and a dynamic reaction field that is induced by interaction of the inner region charge distribution with the dielectric. A great advantage of the GSBP is the possibility to handle irregularly shaped dielectric boundaries. The GSBP was first applied successfully in classical simulations.[34,35] It was later adapted for use in combination with a hybrid QM/MM Hamiltonian,[20] with the self-consistent-charge density-functional tight-binding (SCC-DFTB) method[36] as the QM component. The resulting SCC-DFTB/MM/GSBP approach proved to be efficient and accurate and was applied in several studies of biological systems.[37−40] It was only found to be problematic in one case where the macromolecule underwent major conformational changes.[41] Since the fixation of the outer region is the fundamental assumption that allows for a closed-form expression for the electrostatics, the GSBP is not adequate to study nonlocal processes. Recently, the GSBP was implemented for NDDO-based semiempirical QM/MM Hamiltonians, and an evaluation showed that the GSBP allows accurate semiempirical QM/MM MD simulations at significantly reduced computational costs compared to standard QM/MM methods.[21]

Although semiempirical QM/MM MD simulations enable sufficient sampling of phase space, they suffer from the inaccuracies of the semiempirical QM Hamiltonian. As QM/MM MD simulations with accurate density functional or ab initio methods are prohibitively expensive, several schemes have been devised to approximate free energy differences on the basis of first-principles quantum mechanics.[1,8,42−50] The QM/MM free energy perturbation (FEP) method[51] is one of these approaches. It is based on three assumptions: (1) the dynamics of the QM and MM subsystems are independent; (2) the entropy change in the QM region can be estimated from the harmonic approximation, and (3) commonly, the electrostatic QM/MM interactions are approximated by interactions between QM and MM point charges, with the QM charges fitted to the electrostatic
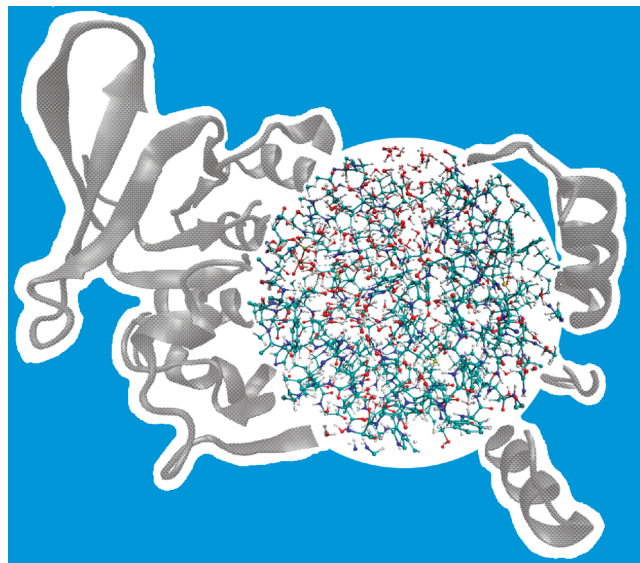
Figure 1. Illustration of the boundary potential approach. The explicit inner region is represented atomistically. The implicit outer macromolecule region is depicted by gray ribbons, and the implicit solvent region is represented by the blue area.

potential (ESP).[2] These approximations reduce the computational costs significantly such that computation of free energy differences is possible with accurate QM/MM methods. The validity of this approach is supported by successful applications[3,52−54] and comparisons to nonapproximated free energy methods.[7,10]

In this article, we present a general boundary potential for QM/MM calculations that offers two new possibilities. First, it extends the QM/MM method to a general three-layer approach that describes the outer solvent and macromolecule region by a boundary potential and thus allows for an accurate description of long-range electrostatic interactions and bulk solvent effects. Second, within the FEP framework, it allows application of the GSBP to sample the MM phase space more efficiently. Both options are available in combination with every QM/MM potential. Since this boundary potential mimics the electrostatic potential of the outer region of macromolecules in solution, we denote it the solvated macromolecule boundary potential (SMBP).

2. Methods

This section begins with a definition of the different regions into which the full system is separated using a boundary potential approach. Then, the theory of the GSBP is briefly reviewed, and the new SMBP for QM/MM calculations is introduced. Finally, we show how the combined use of the SMBP and GSBP allows efficient ab initio QM/MM free energy calculations within the FEP framework.

2.1. Separation of Regions. The foundation of any boundary potential approach is the separation of the full system into an inner and outer region. This partitioning is illustrated in Figure 1. All atoms in the inner region (colored atomistic representation) are simulated explicitly, while the influence of the outer region (shown in gray ribbons) on the inner region is mimicked by the boundary potential.

The atoms in both regions interact with the dielectric continuum that represents the bulk solvent (blue area).

Considering a macromolecule R surrounded by N solvent molecules in a boundary potential approach, the inner region comprises the inner part of the macromolecule (R_i) and the n inner solvent molecules, while the outer $N - n$ solvent molecules and the outer part of the macromolecule (R_o) belong to the outer region. Statistical expectation values depending only on the degrees of freedom of the inner region can be computed on the surface of the potential of mean force (PMF) $W(R_i, 1, ..., n)$.

$$e^{-\beta W(R_i,1,...,n)} = \frac{1}{C} \int' dR_o \, d(n+1) \cdots dN e^{-\beta U(R,1,...,N)}$$
(1)

The PMF is obtained by integrating out the degrees of freedom of the outer region, including only those configurations with all outer region atoms outside the inner region (as indicated by the primed integral). Beglov and Roux demonstrated that the PMF is related to the reversible thermodynamic work necessary to assemble the inner region if the integration constant C is chosen accordingly.[33] This allows separation of the PMF into contributions that arise from configurational restrictions (ΔW_{cr}), nonpolar interactions (ΔW_{np}), electrostatic interactions (ΔW_{elec}), and the potential energy of the isolated inner region (U).

$$W(R_i, 1, ..., n) = U(R_i, 1, ..., n) + \Delta W_{cr} + \Delta W_{np}(R_i, 1, ..., n) + \Delta W_{elec}(R_i, 1, ..., n)$$
(2)

Although the accuracy of the GSBP and the SMBP decreases in the immediate vicinity of the boundary, it is important to ensure that the inner region preserves its shape. Therefore, it is necessary to fix the outer layer of the inner region.[21] As a consequence, the inner region is further subdivided into an active explicit and a frozen explicit region.

2.2. Generalized Solvent Boundary Potential. The objective of the GSBP is to provide an efficient and accurate approximation of the electrostatic contribution to the PMF. Hence, the outer solvent molecules are described by a PDC and the outer macromolecule region by fixed point charges. In this case, the electrostatic contributions to the PMF consist of direct Coulombic interactions of the inner and outer regions (U_{elec}^{io}), and the solvation free energy resulting from interaction with the PDC (ΔW_{elec}^{solv}). This term stems from the interaction of the charge distribution of the entire macromolecule, represented by point charges q_A, with the reaction field potential $\phi_{rf}(\mathbf{r})$.

$$\Delta W_{elec}^{solv} = \frac{1}{2} \sum_A q_A \, \phi_{rf}(\mathbf{r}_A)$$
(3)

The reaction field potential is the difference of the electrostatic potentials in solution and in vacuum that are computed by solving the linearized PB equation.[55]

$$\nabla[\varepsilon(\mathbf{r}) \nabla\phi(\mathbf{r})] - \bar{\kappa}^2(\mathbf{r}) \, \phi(\mathbf{r}) = -4\pi\rho(\mathbf{r})$$
(4)

Here, $\rho(\mathbf{r})$ is the charge density, $\varepsilon(\mathbf{r})$ is the space-dependent dielectric constant, and $\bar{\kappa}(\mathbf{r})$ is the modified Debye–Hückel screening factor. Direct computation of this term during sampling is prohibitively expensive since it would require solving the PB equation for each configuration. To isolate the dynamic contributions, the charge distribution is separated into an inner and outer part, and as a consequence ΔW_{elec}^{solv} splits up into outer–outer, inner–outer, and inner–inner contributions.

$$\Delta W_{elec}^{solv} = \Delta W_{elec}^{oo} + \Delta W_{elec}^{io} + \Delta W_{elec}^{ii}$$
(5)

The interaction of the outer region charge distribution with the self-induced reaction field (ΔW_{elec}^{oo}) is constant throughout sampling and can therefore be neglected. Calculation of the direct Coulombic interactions of the inner and outer regions and the inner–outer contribution to the solvation free energy can be combined efficiently.

$$\Delta W_{elec}^{io} + U_{elec}^{io} = \sum_{A \in inner} q_A \, \phi_{rf}^o(\mathbf{r}_A) + U_{elec}^{io}$$
$$= \sum_{A \in inner} q_A \phi_s^o(\mathbf{r}_A)$$
(6)

Since the outer region is constant, the electrostatic potential of the outer region in solution, ϕ_s^o, is constant for all inner region configurations, and therefore, this ansatz offers a massive reduction of computational cost. The inner–inner contributions, however, remain problematic since the inner reaction field potential depends on the inner region configuration. To find an analytical expression for this term, a Green's function approach is used to express the inner reaction field potential.

$$\phi_{rf}^i(\mathbf{r}) = \int d\mathbf{r}' \, \rho_i(\mathbf{r}') \, G_{rf}(\mathbf{r}, \mathbf{r}')$$
(7)

Now, the inner charge distribution and the reaction field Green's function are projected onto the same set of basis functions $\{b_n\}$, and the solvation energy of the inner region can be expressed as a matrix product of the reaction field matrix, M_{rf}, and the generalized multipole moments of the inner charge distribution, Q_n. This leads to the final expression for the electrostatic contribution to the PMF.

$$\Delta W_{elec}^{GSBP} = \sum_{A \in inner} q_A \phi_s^o(\mathbf{r}_A) + \frac{1}{2} \sum_{mn} Q_m M_{mn} Q_n$$
(8)

Although this ansatz circumvents repeated solution of the PB equation during sampling, it is important to point out that computation of the reaction field matrix necessitates solving the PB equation a few hundred times before the simulation. Therefore, use of the GSBP is connected with a significant overhead.[21]

In the QM/MM approach, the inner region is subdivided into a QM and a MM region, and concomitantly, the inner region charge distribution splits up into QM and MM charge distributions that interact separately with the static outer region potential, ϕ_s^o, and the reaction field Green's function, G_{rf}.

$$\Delta W_{\text{elec}}^{\text{GSBP}} = \sum_{A \in \text{MM}} q_A \phi_s^o(\mathbf{r}_A) + \int d\mathbf{r}\, \rho^{\text{QM}}(\mathbf{r})\, \phi_s^o(\mathbf{r}) +$$
$$\frac{1}{2} \sum_{mn} Q_m^{\text{QM}} M_{mn} Q_n^{\text{QM}} + \sum_{mn} Q_m^{\text{QM}} M_{mn} Q_n^{\text{MM,cs}} +$$
$$\frac{1}{2} \sum_{mn} Q_m^{\text{MM}} M_{mn} Q_n^{\text{MM}}$$

$$(9)$$

The charge-shift scheme is employed to avoid overpolarization of the QM electron density, by distributing the charges of MM atoms at the QM/MM boundary over the neighboring MM atoms and correcting for the resulting change in the dipole moment.[56] Therefore, the QM multipole moments (Q_m^{QM}) interact with the multipole moments of the charge-shifted MM charge distribution ($Q_n^{\text{MM, cs}}$) via the reaction field matrix (M_{mn}).

The main issue of any QM/MM implementation of the GSBP is the representation of the continuous QM charge density, $\rho^{\text{QM}}(\mathbf{r})$. In previous implementations,[20,21] the QM density was represented by Mulliken charges.[57]

$$\rho^{\text{QM}}(\mathbf{r}) = \sum_A q_A^{\text{Mulliken}}(\mathbf{r}_A)\, \delta(\mathbf{r} - \mathbf{r}_A) \qquad (10)$$

This choice has the two advantages that the working equations of the GSBP for MM methods can be easily extended to the QM/MM case and that the interaction of the QM density with the boundary potential during the self-consistent field (SCF) procedure can be expressed in simple terms that have to be added to the Fock matrix. However, there are also two disadvantages. First, the GSBP has to be implemented for each QM program and method individually. Second, to compute accurate analytical gradients, it is necessary to calculate the derivative of the Mulliken charges, which involves solution of the coupled-perturbed SCF (CPSCF) equations. While the computational costs of this step are acceptable for semiempirical methods, they will increase significantly for higher-level QM methods with larger atomic orbital basis sets.[21]

2.3. Solvated Macromolecule Boundary Potential. The design of the SMBP was guided by the requirements that it should be conceptually similar to the GSBP, efficient in geometry optimizations, and applicable in QM/MM calculations with any kind of QM method.

We first consider the definition of the dielectric boundary: The core of the GSBP is the analytical expression for the electrostatic interaction with the outer region charge distribution that is shielded in a nontrivial way by the PDC. To find a closed-form expression for this potential, it is necessary to assume that the dielectric interface is fixed during the simulation.[34] Usually, in solutions of the PB equation, the interface is defined by the superposition of the van der Waals (vdW) envelope of the atoms. In the GSBP, a constant and smooth dielectric interface throughout dynamics simulations is ensured by extending the dielectric cavity region that encloses the inner region. For the sake of consistency, the same approach is used in the SMBP. The inner region is restricted to have a spherical shape with radius R_{inner} that comprises all inner region atoms. Since all atoms inside the sphere are modeled explicitly, the dielectric constant inside
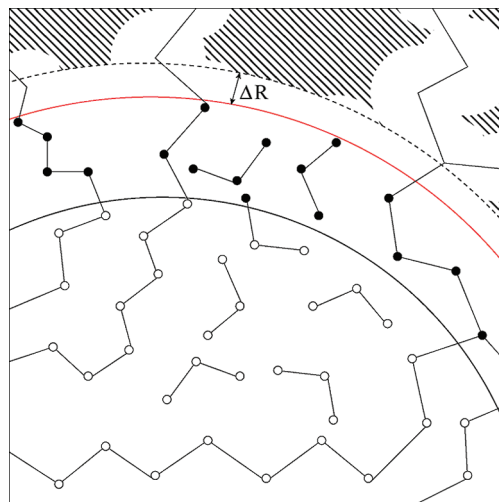
Figure 2. Definition of the constant dielectric interface in the SMBP and the GSBP. The extended cavity region is encircled by the dashed black line, and the implicit solvent region is indicated by the hatched area. An "insulation" region of frozen explicit atoms (black circles) ensures (see text) that the dielectric interface is not touched by the van der Waals radius of any active explicit atom (white circles). The inner region and the active region are encircled by red and black lines, respectively.

the inner region is set to 1. In the bulk solvent and the macromolecule region, the dielectric constant is set to ε_s and ε_m, respectively. To secure that the shape of the interface is independent of the position of the active atoms, the radius of the inner region cavity is extended by ΔR. This value has to be chosen to be sufficiently large to avoid the vdW radius of any active atom touching the interface. The resulting shape of the dielectric interface in the SMBP is illustrated in Figure 2. A previous evaluation of the GSBP showed that its accuracy deteriorates close to the boundary of the inner region.[21,35] Therefore, it was found necessary to freeze the outer layer of the inner region, providing an "insulation" region with a thickness of 2−3 Å.[21] In Figure 2, this is the area between the red and black line. Here, the atoms are described explicitly, but their positions are fixed.

The construction of the SMBP is based on the same approximations as in the case of the GSBP. Outer macromolecule and bulk solvent regions are represented by fixed point charges and a PDC, respectively, so that the electrostatic contributions to the PMF consist of direct Coulombic interactions ($U_{\text{elec}}^{\text{io}}$) and the solvation free energy ($\Delta W_{\text{elec}}^{\text{solv}}$). Again, the outer−outer contribution to the solvation free energy is constant and therefore neglected, so that the SMBP takes the following form:

$$\Delta W_{\text{elec}}^{\text{SMBP}} = U_{\text{elec}}^{\text{io}} + \Delta W_{\text{elec}}^{\text{io}} + \Delta W_{\text{elec}}^{\text{ii}} \qquad (11)$$

As in the GSBP, the electrostatic interactions of the inner region with the outer region charges ($U_{\text{elec}}^{\text{io}}$) and with the response of the PDC to the outer region charges ($\Delta W_{\text{elec}}^{\text{io}}$) are combined for efficient computation (eq 6).

$$\Delta W_{\text{elec}}^{\text{SMBP}} = \int d\mathbf{r}\, \rho_i(\mathbf{r})\, \phi_s^o(\mathbf{r}) + \Delta W_{\text{elec}}^{\text{ii}} \qquad (12)$$

In the GSBP, ΔW_{elec}^{ii} is approximated by a closed-form expression that is based on a basis set representation of the inner region charge distribution and the reaction field Green's function (see eqs 7 and 8). This approach is designed for MD simulations but is computationally not efficient for geometry optimizations or single-point calculations. Using a standard-sized basis set to represent the charge density, computation of the reaction field matrix corresponds to solving the PB equation about 800 times. Even with a large active region, geometry optimizations rarely take more than than 800 steps to converge, and therefore solving the PB equation after each step is more efficient. Since geometry optimizations are the field of application of the SMBP, we use a different ansatz and update the individual contributions to the PMF by solving the PB equation whenever needed. This is the main conceptual difference between SMBP and GSBP.

In the QM/MM/SMBP approach, the inner region charge distribution splits up into QM and MM charge densities, leading to a more complicated expression.

$$\Delta W_{elec}^{SMBP} = \frac{1}{2} \int d\mathbf{r} \, d\mathbf{r}' [\rho_{QM}(\mathbf{r}) + \rho_{MM}(\mathbf{r})] \times$$
$$G_{rf}(\mathbf{r}, \mathbf{r}')[\rho_{QM}(\mathbf{r}') + \rho_{MM}(\mathbf{r}')] + \qquad (13)$$
$$\int d\mathbf{r}[\rho_{QM}(\mathbf{r}) + \rho_{MM}(\mathbf{r})] \, \phi_s^o(\mathbf{r})$$

This can also be formulated as the interaction with the individual potentials ϕ_{tot}^{QM} and ϕ_{tot}^{MM} that are experienced by the QM and MM charge densities, respectively:

$$\Delta W_{elec}^{SMBP} = \int d\mathbf{r} \, \rho_{QM}(\mathbf{r}) \, \phi_{tot}^{QM}(\mathbf{r}) + \int d\mathbf{r} \, \rho_{MM} \, \phi_{tot}^{MM}(\mathbf{r}) \qquad (14)$$

with

$$\phi_{tot}^{QM}(\mathbf{r}) = \phi_s^o(\mathbf{r}) + \phi_{rf}^{MM}(\mathbf{r}) + \frac{1}{2}\phi_{rf}^{QM}(\mathbf{r}) \qquad (15)$$

$$\phi_{tot}^{MM}(\mathbf{r}) = \phi_s^o(\mathbf{r}) + \frac{1}{2}\phi_{rf}^{MM}(\mathbf{r}) \qquad (16)$$

Both inner region reaction field potentials, ϕ_{rf}^{QM} and ϕ_{rf}^{MM}, are computed by solving the PB equation in solution and in a vacuum with all charges set to zero except the explicit QM and MM charges, respectively (see eq 4). Since ϕ_{rf}^{QM} and ϕ_{rf}^{MM} depend on the inner region charge distributions, they have to be calculated for each inner region configuration, that is, after each step in a geometry optimization.

Moreover, computation of the QM reaction field potential is exacerbated by the mutual dependence of the QM wave function and the QM reaction field potential via the QM charge density. To find a self-consistent solution to the SCF and the PB equation at the same time, a doubly iterative self-consistent reaction field (SCRF) scheme is employed.

In previous implementations of the GSBP for QM/MM methods, the interaction of the QM charge density was modeled by QM Mulliken charges interacting with the boundary potential. Although this leads to simple additional terms that have to be added to the Fock matrix, it also necessitates modifications to the QM programs.[20,21] In accordance with the modular philosophy of ChemShell, a
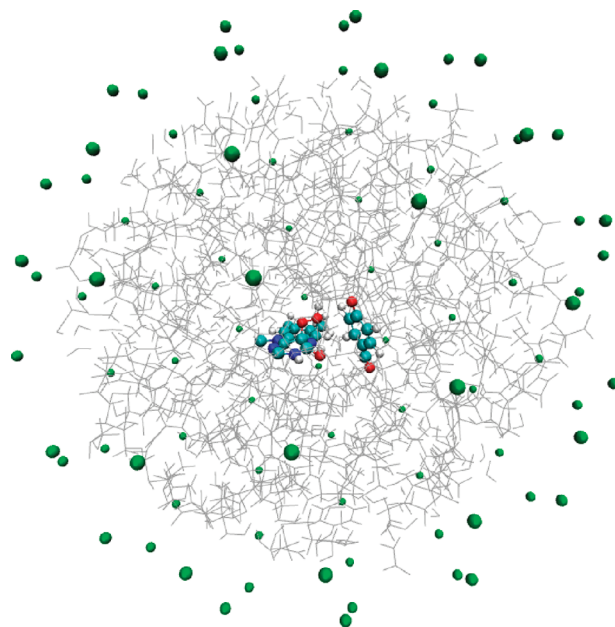
Figure 3. Distribution of virtual surface charges used to represent the SMBP (green balls) in the case of *p*-hydroxybenzoate hydroxylase (see section 4.2). The QM region and the explicit MM region are shown as a ball-and-stick model and as gray lines, respectively.

different approach is used in the SMBP to describe the interaction of the QM charge density with the boundary potential. The boundary potential is projected onto a set of N virtual surface charges $\{q_i\}$, which are distributed uniformly on a sphere with radius $R_{inner} + \Delta R$ that defines the extended dielectric cavity (see Figure 3).

$$\phi_{tot}^{QM}(\mathbf{r}) \approx \sum_i^N \frac{q_i}{|\mathbf{r} - \mathbf{r}_i|} \qquad (17)$$

The values of the surface charges are optimized to reproduce ϕ_{tot}^{QM} at the position of the QM atoms by minimization of the penalty function $\tilde{F}$.

$$\tilde{F} = \sum_j^{QM} \left[\phi_{tot}^{QM}(\mathbf{r}_j) - \sum_i^N \frac{q_i}{|r_{ij}|} \right]^2 \qquad (18)$$

The minimization of $\tilde{F}$ starts with all virtual surface charges set to zero. The charges are optimized with a conjugate gradient algorithm until ϕ_{tot}^{QM} is reproduced with a maximum absolute deviation of 2×10^{-5} au at the position of every QM atom. The QM wave function is optimized in the presence of the atomic charges of the inner MM region and the virtual surface charges. The surface charge projection approach has the advantage of allowing the application of the SMBP in combination with every QM program that can handle external point charges.

For each new geometry, the MM reaction field potential ϕ_{rf}^{MM} is computed by neglecting all charges in the outer region and the QM region. Since the MM charges are not polarizable and the potential is independent of the QM charge distribution, the MM reaction field does not have to be updated due to changes in the QM density. Subsequently, a SCRF calculation proceeds as follows: (1) Initially, the QM reaction

field potential ϕ_{rf}^{QM} is computed on the basis of a guess for the atomic QM charges. (2) Then, the total potential experienced by the QM atoms, ϕ_{tot}^{QM}, is assembled and projected onto a set of virtual surface charges $\{q_i\}$. (3) ==Next, the QM wave function is computed in the field of the inner MM region point charges and the surface charges.== After convergence, the QM ESP charges based on the new wave function are calculated. (4) With these new QM charges, the PB equation is solved again to update the QM reaction field potential. (5) Finally, the potential is checked for convergence. If the deviations in the QM reaction field potential are too large, the algorithm returns to step 2 and updates the wave function and the QM reaction field potential. (6) Upon convergence, the force contributions from the total potential are computed and added to the gradient.

These force contributions are the derivative of the electrostatic contribution to the PMF with respect to the atomic coordinates. For a QM atom, this yields

$$
\begin{aligned}
\frac{\partial}{\partial x_A}\Delta W_{elec}^{SMBP} = \; & \frac{\partial}{\partial x_A}\frac{1}{2}\int d\mathbf{r}\, d\mathbf{r}'\, \rho_{QM}(\mathbf{r})\, G_{rf}(\mathbf{r},\mathbf{r}')\, \rho_{QM}(\mathbf{r}') + \\
& \frac{\partial}{\partial x_A}\int d\mathbf{r}\, d\mathbf{r}'\, \rho_{QM}(\mathbf{r})\, G_{rf}(\mathbf{r},\mathbf{r}'\, \rho_{MM}(\mathbf{r}') + \\
& \frac{\partial}{\partial x_A}\int d\mathbf{r}\, \rho_{QM}(\mathbf{r})\, \phi_s^o(\mathbf{r}) \\
= \; & \int d\mathbf{r}\left[\frac{\partial}{\partial x_A}\rho_{QM}(\mathbf{r})\right]\phi_{tot}^{grad}(\mathbf{r})
\end{aligned}
$$

(19)

with

$$
\phi_{tot}^{grad}(\mathbf{r}) = \phi_s^o(\mathbf{r}) + \phi_{rf}^{MM}(\mathbf{r}) + \phi_{rf}^{QM}(\mathbf{r}) \qquad (20)
$$

Projection of the total gradient potential ϕ_{tot}^{grad} onto a set of K gradient surface charges $\{q_p\}$ leads to the following approximation:

$$
\frac{\partial}{\partial x_A}\Delta W_{elec}^{SMBP} \approx \int d\mathbf{r}\left[\frac{\partial}{\partial x_A}\rho_{QM}(\mathbf{r})\right]\left[\sum_p^K \frac{q_p}{|\mathbf{r}_p - \mathbf{r}|}\right]
$$

(21)

These terms are computed and added to the QM gradient automatically by every standard quantum chemistry code if the QM gradient calculation is performed in the presence of a set of point charges that encompasses the point charges of the inner MM atoms and the gradient surface charges. For SCF wave functions, solution of the CPSCF equations is not necessary for gradient computations, since all terms involving derivatives of variationally optimized orbital coefficients are zero. In the QM/MM/SMBP approach, however, the Fock matrix in the gradient calculation is not strictly diagonal because the virtual surface charges are different in the energy and the gradient calculations (see eqs 15 and 20). Thus, the QM wave function is not converged in the field of the gradient surface charges. However, the QM contribution to the total gradient potential is very small, and the differences between virtual surface charges for energy and gradient calculations are therefore almost zero. By comparison to finite-difference gradient calculations, we found that all terms involving orbital coefficient derivatives can be neglected in

geometry optimizations with standard convergence criteria (see Table S1 in the Supporting Information). If the dielectric constant of the solvent region is 1, that is, in case of a calculation in vacuo, all reaction field contributions are zero, and the analytical gradient is exact within the QM/MM/SMBP approximation. In summary, the potential projection approach offers a two-fold advantage: First, the SMBP can be used in combination with every quantum chemistry code, and second, solution of the CPSCF equation can be avoided for all practical purposes. Conceptually similar SCRF procedures have been used previously to combine pure QM[58] and hybrid QM/MM approaches[59] with implicit solvation models. The method presented in this work extends upon these approaches and employs a combination of the SCRF procedure and virtual surface charges to compute and represent a boundary potential that mimics not only the implicit solvent but also the outer macromolecule region.

For an MM atom, the derivative takes a similar form:

$$
\frac{\partial}{\partial x_A}\Delta W_{elec}^{SMBP} = \int d\mathbf{r}\left[\frac{\partial}{\partial x_A}\rho_{MM}(\mathbf{r})\right]\phi_{tot}^{grad}(\mathbf{r}) \qquad (22)
$$

As the MM charges are constant, the derivative of the MM charge distribution is just the derivative of the function that is used to distribute the MM charges onto the grid employed for solving the PB equation.[60]

2.4. QM/MM/GSBP-FEP Approach. Since the QM/MM-FEP approach has been presented in detail previously,[2,10] we discuss it only briefly to explain how the SMBP makes it possible to use the QM/MM/GSBP method for all QM/MM Hamiltonians.

In the FEP approach, the free energy difference is divided into three contributions that are computed individually:

$$
\Delta A = \Delta E_{QM} + \Delta A_{QM/MM} + (\Delta A_{QM} - \Delta E_{QM}) \qquad (23)
$$

At first, the potential energy profile is calculated by means of constrained optimizations. A reaction coordinate ξ describing the reaction is defined and used to split the reaction into discrete windows characterized by a corresponding value of ξ_i. For each window i, the reaction coordinate is constrained to some ξ_i, and all other QM and MM degrees of freedom are optimized. This yields the potential energy profile of the reaction and a set of geometries along the reaction coordinate.

Next, the difference of the free QM/MM interaction energy, $\Delta A_{QM/MM}^{i \to i+1}$, between every two adjacent windows i and $i + 1$ is calculated. The difference is computed as a "perturbation" of the structure of window i with the QM structure of window $i + 1$.

$$
\Delta E_{pert}^{i \to i+1} = E_{QM/MM}(\mathbf{r}_{QM}^{i+1}, \mathbf{r}_{MM}^i) - E_{QM/MM}(\mathbf{r}_{QM}^i, \mathbf{r}_{MM}^i) \qquad (24)
$$

The change in the free energy that corresponds to the perturbation of the QM structure is obtained by sampling over the MM phase space at window i. This means that the MM forces refer to the interaction with the QM structure of window i, which is frozen during sampling.

$$\Delta A_{QM/MM}^{i \to i+1} = -\frac{1}{\beta} \ln \langle \exp(-\beta \Delta E_{pert}^{i \to i+1}) \rangle_{MM,i} \qquad (25)$$

Here, β is $1/(k_B T)$, with k_B being the Boltzmann constant. Using the electronic embedding scheme,[61] an exact calculation of the electrostatic QM/MM interactions necessitates solving the SCF equations for each MM configuration during sampling. In the QM/MM-FEP approach, computation of these interactions is drastically simplified by two assumptions: the QM density is frozen and approximated by atomic ESP charges. Therefore, all QM calculations are avoided during sampling.

Finally, the energy of the QM part is corrected for entropic effects. At the stationary points, the correction ($\Delta A_{QM} - \Delta E_{QM}$) is evaluated from harmonic frequency calculations of the QM atoms and standard methods from statistical thermodynamics.[2,62]

The SMBP allows computation of the potential energy profile and the molecular and electronic structures of the discrete windows with the same approximations as in the GSBP. The outer region solvent molecules are represented by a PDC and the outer macromolecule charges by fixed point charges. The explicit atoms do not interact directly with all outer region charges but only with the potential that is induced by these charges in interaction with the PDC. This potential is computed as the finite-difference solution to the PB equation and is saved on a grid, which allows massive computational savings. Therefore, the geometries, QM densities, and ESP charges that result from (constrained) geometry optimizations with the QM/MM/SMBP method can be used for sampling the free energy difference over the MM phase space with the GSBP. At this point, it seems adequate to highlight the complementary nature of the approximations in QM/MM-FEP and in the GSBP. The QM/MM-FEP ansatz reduces the problem of configurational sampling with a QM/MM Hamiltonian to a sampling over MM phase space with a classical MM method. The GSBP enhances the efficiency of classical MM simulations by representing the outer part of the system by a boundary potential. Hence, these two approaches complement each other and may be combined without a loss of efficiency. Also in the GSBP, the QM density is represented by the ESP charges, leading to simple expressions for the QM multipole moments and the interaction with the static outer region potential.

$$Q_n^{QM} = \sum_{A \in QM} q_A^{ESP} b_n(\mathbf{r}_A) \qquad (26)$$

$$\int d\mathbf{r}\, \rho^{QM}(\mathbf{r})\, \phi_s^o(\mathbf{r}) = \sum_{A \in QM} q_A^{ESP} \phi_s^o(\mathbf{r}_A) \qquad (27)$$

Since values and positions of the ESP charges are different for windows i and $i + 1$, the GSBP will contribute to the QM/MM energy difference that is sampled in eq 25. As the QM atoms are fixed, computation of the QM gradient in interaction with the GSBP is not necessary. The MM gradient is calculated in analogy to other QM/MM/GSBP implementations.[20,34]

3. Computational Details

The SMBP was implemented in a developmental version of the modular program package ChemShell.[56,63] The energy

and gradient evaluations for the QM part were performed with the MNDO[64] and Turbomole 5.7.1 programs.[65] For the MM part, the DL_POLY[66] code was employed to run the CHARMM22 force field in all calculations.[67] Hydrogen link atoms in combination with the charge-shift scheme[56] were applied to saturate the QM system. Stationary points were optimized in hybrid delocalized internal coordinates using the HDLCOpt optimizer.[68] The PB equation was solved with the ChemShell PB module that uses the optimal successive over-relaxation method in combination with Gauss-Seidel relaxation to compute the electrostatic potential.[69,70] A maximum absolute change in every grid point of 2×10^{-5} au was employed as a convergence criterion. Third-order B splines were used to interpolate between the grid points.[71] The definition of the dielectric boundary was based on vdW radii from the CHARMM22 force field. All MD simulations were performed under NVT conditions at a temperature of 300 K, which was controlled by a Nosé-Hoover chain thermostat.[72−75] The mass of deuterium was assigned to all hydrogen atoms, and free water molecules were kept rigid with SHAKE constraints.[76] A time step of 1 fs was used. The QM reaction field potential was considered converged when the root-mean-squared deviation dropped below 2×10^{-5} au. In the first iteration of the SCRF procedure, all QM atoms were assumed to be neutral.

4. Results

In this section, we evaluate the performance of the SMBP using three test cases: the proton transfer reaction in solvated glycine, the hydroxylation reaction in *p*-hydroxybenzoate hydroxylase (PHBH), and the spin state energy gaps in cytochrome P450cam. Glycine surrounded by explicit water molecules is a highly flexible and polar system, which makes it a challenging test case: the reaction energy of the intramolecular proton transfer is sensitive to the description of the solvent, and many solvation models incorrectly predict the neutral form to be more stable than the zwitterionic form.[77−80] The hydroxylation reaction in the catalytic cycle of PHBH has been much studied theoretically[9,81−85] and has become a prototypical test system for benchmarking theoretical treatments of enzymatic reactions.[12] The relative spin state energies of cytochrome P450cam[86,87] provide another, rather different test case: here, we address the pentacoordinated ferric complex whose spin state energies are strongly affected by the protein environment.[88] Taken together, we thus have three diverse systems to evaluate the accuracy and range of applicability of the SMBP.

Previous studies indicate that it may sometimes be important to allow fluctuations in the number of solvent molecules in approaches based on inner regions of fixed size.[89,90] This should not be problematic in the present test calculations, which address localized events at the center of the inner region (using a fixed number of solvent molecules).

4.1. Glycine in Water. The glycine/water model system was set up using a commonly applied protocol of solvation and equilibration steps by means of classical MD simulations with the CHARMM program.[91] The glycine molecule was solvated in a TIP3P water ball with 30 Å radius. All water molecules with an oxygen atom within 2.8 Å of any glycine

atom were deleted, and the system was equilibrated. These steps were repeated until the number of water molecules was stable, leading to a total system size of 12 769 atoms with 4253 TIP3P water molecules. Finally, the system was equilibrated by means of a 500 ps classical MD simulation, and five configurations were selected after 340, 380, 420, 460, and 500 ps. For each configuration, the inner region was centered on the C_α carbon of the glycine and defined to encompass all water molecules with any atom within 18 Å of the center. In all subsequent QM/MM geometry optimizations, the glycine molecule and all water molecules with any atom within 14 Å of the center were allowed to move, while all other water molecules were frozen. The radius of the extended dielectric cavity was set to 21 Å, and a set of 90 virtual surface charges was used to represent the boundary potential in the QM calculations. The glycine molecule was described quantum mechanically with the AM1 Hamiltonian,[92] and the water molecules were treated by the force field or the SMBP. The details of this setup are summarized in Table S2 (Supporting Information).

In a vacuum environment, that is, with a dielectric constant of 1 anywhere in space, the electrostatic potential of the SMBP has to be identical to the exact potential from Coulombic electrostatics. Therefore, the accuracy of the QM/MM/SMBP approach can be evaluated in vacuo by direct comparison to standard QM/MM calculations. To allow the use of finely spaced grids in the finite-difference solution of the PB equation also for large biomolecules, we employed a focusing approach.[93] The PB equation is first solved with a coarse outer grid that covers the full biomolecule. Then, the PB equation is solved again with a fine inner grid that focuses onto the inner region. The boundary values of the inner grid are set by interpolation from the outer grid. The spacings of the two grids are the most important parameters of the SMBP. Hence, the accuracy of the SMBP was evaluated for all mesh size combinations of 0.15, 0.25, 0.4, 0.6, and 0.8 Å for the inner grid and 0.80, 1.25, 1.50, 1.75, and 2.50 Å for the outer grid.

Tables 1 and 2 show the mean absolute (MAD) and maximum absolute deviations (MAX) of the components of the electrostatic gradient for configuration 1. Similar deviations were observed for the other configurations (see Tables S3 and S4 in the Supporting Information). Although only 90 virtual surface charges are used to represent the static potential that is induced by almost 10 000 atoms in the outer region, the electrostatic gradient at the position of the QM atoms is reproduced with high accuracy. For all mesh size combinations, the MAD and MAX values are on the order of 0.3×10^{-4} au and 1.6×10^{-4} au, respectively. Moreover, the accuracy seems to be independent of the grid spacing within the chosen limits. Both findings suggest that the static outer region potential varies only slowly and has no detailed structure in the QM region.

Considering all atoms within 16 Å of the center, the SMBP reproduces the gradient of the electrostatic potential with high accuracy if the spacing of the inner grid is ≤0.4 Å. Under these conditions, the MAX values are below 4×10^{-4} au. The spacing of the outer grid does not influence the accuracy unless very fine inner grids are used. As one approaches the

Table 1. Mean Absolute Deviations (MAD) [10^{-4} au] of the Electrostatic Forces Computed with the SMBP for Configuration 1 of the Glycine/Water System[a]

outer grid size [Å]	inner grid size [Å]				
	0.15	0.25	0.40	0.60	0.80
	MAD - QM atoms				
0.80	0.31	0.31	0.31	0.32	0.31
1.25	0.31	0.31	0.31	0.31	0.31
1.50	0.35	0.32	0.33	0.33	0.33
1.75	0.33	0.32	0.32	0.32	0.32
2.50	0.33	0.34	0.34	0.34	0.33
	MAD - atoms within 16 Å				
0.80	0.18	0.10	0.15	0.20	0.26
1.25	0.21	0.15	0.19	0.23	0.28
1.50	0.28	0.21	0.26	0.29	0.34
1.75	0.26	0.19	0.24	0.27	0.32
2.50	0.29	0.23	0.28	0.30	0.35
	MAD - atoms within 20 Å				
0.80	0.23	0.27	0.57	1.02	1.42
1.25	0.28	0.32	0.61	1.04	1.44
1.50	0.37	0.38	0.67	1.09	1.48
1.75	0.34	0.36	0.65	1.08	1.46
2.50	0.38	0.39	0.68	1.10	1.48

[a] Different mesh size combinations were used.

Table 2. Average Maximum Absolute Deviations (MAX) [10^{-4} au] of the Electrostatic Forces Computed with the SMBP for Configuration 1 of the Glycine/Water System[a]

outer grid size [Å]	inner grid size [Å]				
	0.15	0.25	0.40	0.60	0.80
	MAX - QM atoms				
0.80	1.53	1.64	1.57	1.55	1.60
1.25	1.62	1.69	1.65	1.65	1.67
1.50	1.62	1.66	1.64	1.64	1.66
1.75	1.59	1.65	1.61	1.61	1.64
2.50	1.57	1.63	1.60	1.60	1.62
	MAX - atoms within 16 Å				
0.80	1.53	1.64	3.72	7.16	9.08
1.25	1.67	1.90	3.68	7.08	8.89
1.50	3.22	2.90	3.91	7.30	9.45
1.75	2.32	2.44	3.73	7.14	9.02
2.50	3.15	3.06	3.88	7.19	9.51
	MAX - atoms within 20 Å				
0.80	2.41	5.43	14.79	35.67	35.35
1.25	2.91	5.57	14.59	35.46	35.27
1.50	4.93	5.79	14.53	35.42	34.71
1.75	3.60	5.64	14.52	35.39	35.03
2.50	4.67	5.51	14.25	35.11	34.81

[a] Different mesh size combinations were used.

boundary separating inner and outer regions, the static outer region potential naturally becomes stronger and more complex. Nevertheless, its details are captured with sufficient accuracy also at the position of all inner region atoms which have a distance of up to 20 Å to the center due to the residue-based selection criterion that was employed to define the inner region. With an inner grid spacing of ≤0.25 Å, the MAD values do not exceed 0.4×10^{-4} au, and maximum deviations are around 5.5×10^{-4} au.

The accuracy of the SMBP depends strongly on the radial position of the atoms since the electrostatic potential is more complex at the boundary. Figure 4 illustrates this point and shows that the increase of the MAD and MAX values in proximity to the boundary is strongly affected by the mesh
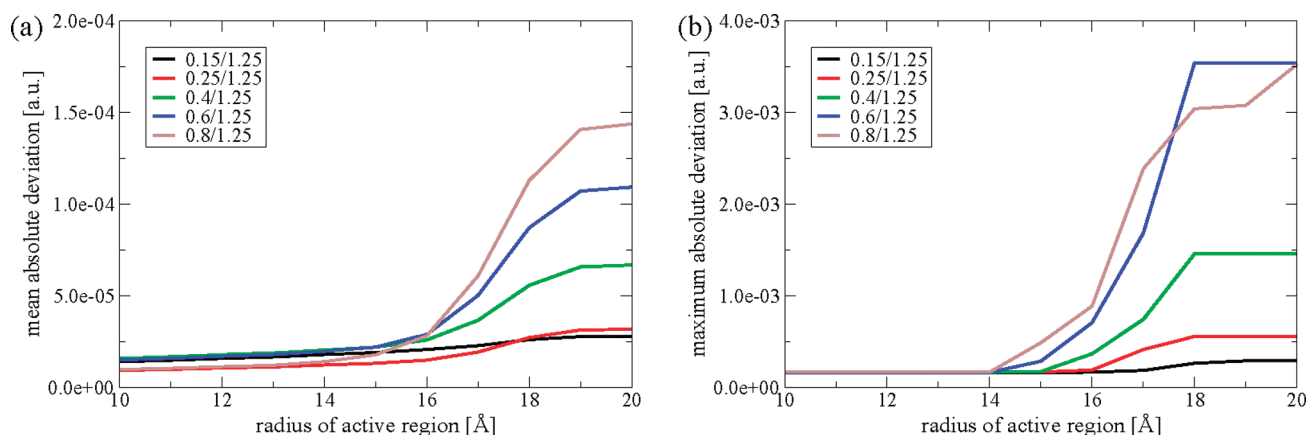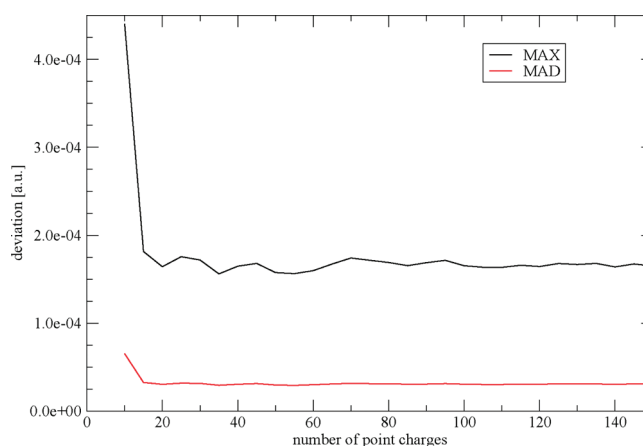
Figure 4. Mean absolute deviations (a) and maximum absolute deviations (b) of the electrostatic forces of all atoms inside the active region relative to the exact QM/MM values. Results are shown for different mesh sizes of the inner grid and plotted as a function of the radius of the active region. An outer grid size of 1.25 Å is used, and all calculations were performed on configuration 1 of the glycine/H_2O test system. The radius of the inner region was 18 Å (see text).

size of the inner grid. The deviations increase only slowly with grid spacings of 0.15 or 0.25 Å, and much more rapidly for coarser inner grids.

Overall, the accuracy provided by the SMBP is sufficient for QM/MM geometry optimizations where the default convergence criterion is a maximum gradient component of 4.5×10^{-4} au.[68] Therefore, an inner grid spacing of 0.25 Å excels as the best choice, providing high accuracy at tolerable computational costs. Using a finer grid spacing of 0.15 Å seems to yield only marginal improvements but raises computational demands significantly. The mesh size of the outer grid has no observable influence on the accuracy. Since computational costs are only slightly affected by the outer grid spacing, we opt for a rather fine outer grid with a mesh size of 1.25 Å in combination with an inner grid spacing of 0.25 Å in all calculations.

Representation of the boundary potential by a small set of point charges in the QM calculations is one of the main approximations connected with the SMBP. The accuracy converges rapidly with respect to the number of point charges, as illustrated in Figure 5. The MAD and MAX deviations of the gradient components are around 0.3×10^{-4} and 1.7×10^{-4} au, respectively, if the number of point charges is greater than 20. The residual error is not caused by the point charge representation but results from the limited accuracy of the boundary potential, which is computed from a finite-difference solution of the PB equation. Similar deviations are encountered for the MM atoms within 16 Å of the center that interact directly with the boundary potential without a charge representation (see Tables 1 and 2). Hence, higher accuracies can only be achieved with finer mesh sizes and not with a higher number of virtual surface charges. A set of 90 point charges was employed for all calculations reported in this article.

Using electronic embedding, computation of QM/MM energies and gradients necessitates evaluation of numerous one-electron integrals and their derivatives with respect to the position of the MM atoms. Therefore, computation of these terms constitutes a significant share of the total computational costs of the QM calculation. The SMBP allows us to replace the numerous outer MM atoms by a


Figure 5. Mean absolute (MAD) and maximum absolute deviations (MAX) of the QM gradient components relative to the exact values from full QM/MM calculations. The results are plotted as a function of the number of point charges that are used to represent the boundary potential in the QM calculations. All calculations were performed on configuration 1 of the glycine/H_2O test system.

small set of point charges that reproduces the electrostatic potential in the QM region. In a vacuum environment, the analytical QM/MM/SMBP gradient is exact, and the additional costs of the SCRF procedure can be avoided. Hence, application of SMBP in vacuo offers a reduction of computational costs for QM/MM geometry optimizations. As in standard QM/MM calculations, the bulk solvent is then modeled by fixed water molecules which contribute to the static outer region potential (ϕ_s^0 in eq 12). Table 3 shows the computation times for the QM part of single-point QM/MM and QM/MM/SMBP energy and gradient evaluations. Timings were performed for three QM methods: the semiempirical AM1 method, the pure density functional BLYP,[94,95] and the hybrid density functional B3LYP.[96] Two different basis sets were employed in the density functional theory calculations: the small SVP[97] and the larger TZVPP[98] basis sets. If the QM calculation is not dominated by the two-electron part, that is, if semiempirical methods, pure functionals, or small basis sets are employed, application of the SMBP can reduce computational costs by up to 60%. Even

Table 3. Computation Time for a Single QM Energy and Gradient Evaluation for the Glycine/Water System[a]

| QM method | basis | computation time [s] | | savings [%] |
		QM/MM	QM/MM/SMBP	
AM1		0.5	0.2	−57
BLYP	SVP	76.8	30.5	−60
B3LYP		87.0	39.5	−54
BLYP	TZVPP	303.1	126.1	−58
B3LYP		542.5	370.5	−31

[a] All timings were computed serially on 2.6 GHz AMD Opteron machines with 16 GB of memory.
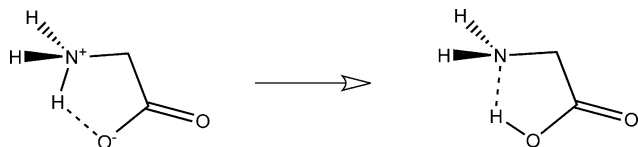
Figure 6. Intramolecular proton transfer reaction in glycine.

for the hybrid B3LYP functional with a larger basis set, computation time is reduced by about 30%. Computational savings strongly depend on the size of the QM region, the inner region and the outer region, and on the QM method employed and can vary significantly for different systems.

The reaction and activation energies for the intramolecular proton transfer process in glycine (Figure 6) were computed using the standard QM/MM and the new QM/MM/SMBP Hamiltonian for the five different configurations. The results in Table 4 show little agreement of QM/MM and QM/MM/SMBP results for the individual configurations. For configurations 3 and 5, deviations of the QM/MM/SMBP results from the QM/MM values are on the order of 1 kcal/mol. Higher deviations of reaction and activation energies up to 6 kcal/mol are encountered for the other configurations. These strong discrepancies can be attributed to the high flexibility and polarity of the system. A closer inspection of the reactant structures revealed that a small number of water molecules at the boundary of the active region adopt a different orientation in the QM/MM/SMBP optimized structures. Due to the hydrogen-bonding network, some of these modifications get relayed to the center of the water sphere and modify the hydrogen-bonding situation in close proximity to the QM region. For this reason, geometry optimizations of the starting structures with the QM/MM and QM/MM/SMBP approach lead to different local minima. Since the relative energies depend on the solvation of the polar groups

of the reactant and product state, the reaction energies vary significantly when starting from different local minima. However, when computations of the reaction profiles are initiated from the same local minimum, that is, by using QM/MM optimized geometries as input structures for QM/MM/SMBP geometry optimizations, both methods provide virtually identical results (see Table 4). This is not practical in applications where QM/MM/SMBP should be used for geometry optimizations but shows that QM/MM/SMBP can reproduce QM/MM results accurately. In summary, for systems with a large number of close-lying local minima that have significantly different characteristics, geometry optimizations using QM/MM and QM/MM/SMBP can yield deviating results because of convergence to different local minima.

The mean values of the reaction and activation energies for the five configurations considered differ by less than 1 kcal/mol between QM/MM and QM/MM/SMBP (Table 4). Moreover, the mean values from QM/MM/SMBP calculations lie within the error bars of the QM/MM mean values (corresponding to a confidence level of 68%), while the standard deviations within the individual data sets range from 3−6 kcal/mol. One may expect in general that the mean values of interest from QM/MM and QM/MM/SMBP optimizations will tend to approach each other for a sufficiently large number of configurations.

4.2. *p*-Hydroxybenzoate Hydroxylase. The setup for PHBH was based on a system that has been used in previous QM/MM studies of PHBH.[9,81,82] It was generated by solvating the enzyme (394 amino acids) containing the flavin-adenine hydroperoxide cofactor (FADHOOH), the dianionic *p*-hydroxybenzoate substrate (pOHB), and 294 crystallographic water molecules in a 90 Å water box. The system was equilibrated with gradually decreasing harmonic restraints on the non-water atoms, followed by a MD run with harmonic restraints acting only on the FADHOOH and pOHB. In the resulting structure that served as a starting point for our setup, all water molecules outside 11 Å from any protein atom were discarded.[9,81,82]

Due to a change of force field from GROMOS (previously) to CHARMM (this study), the system was re-equilibrated for 500 ps with constraints on the cofactor, substrate, and all water molecules outside 2.9 Å from any protein atom. Two configurations were selected from this MD run after 460 and 500 ps that were used as starting structures to locate the stationary points of the hydroxylation reaction. The QM

Table 4. Reaction and Activation Energies for the Proton Transfer Reaction in Solvated Glycine

| configuration | reaction energies [kcal/mol] | | | activation energies [kcal/mol] | | |
	QM/MM	QM/MM/SMBP	QM/MM/SMBP(opt)[a]	QM/MM	QM/MM/SMBP	QM/MM/SMBP(opt)[a]
1	6.84	8.42	6.88	30.01	30.09	30.01
2	9.54	15.61	9.61	32.28	36.43	32.31
3	6.51	7.68	6.61	26.82	27.10	26.84
4	7.27	1.39	7.28	31.18	27.92	31.14
5	13.57	14.58	13.53	32.66	33.35	32.62
mean value	8.75	9.54	8.78	30.73	31.20	30.58
standard deviation of data[b]	2.94	5.77	2.91	2.69	4.46	2.34
standard deviation of mean[c]	1.32	2.58	1.31	1.20	1.99	1.04

[a] Starting from QM/MM optimized structures. [b] Standard deviation of individual energy values. [c] Standard deviation of the mean value (68% confidence limit).
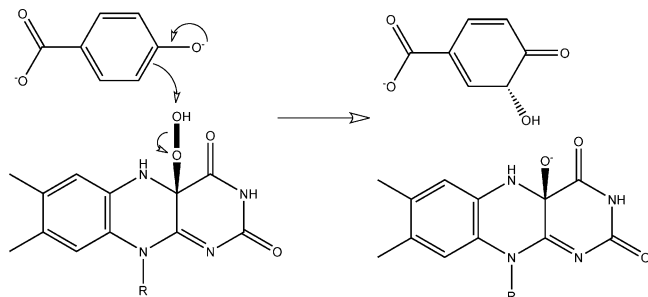
Figure 7. Hydroxylation reaction catalyzed by PHBH. R denotes the ribityl side chain of the flavin cofactor.

Table 5. Potential and Free Energies of Activation and Reaction of the Hydroxylation Reaction in PHBH [in kcal/mol]

| configuration	Hamiltonian	ΔE	$\Delta E^{\ddagger}$	ΔA	$\Delta A^{\ddagger}$
1	QM/MM	−47.44	22.42	−50.38	21.27
	QM/MM/BP[a]	−48.65	21.56	−50.47	20.40
2	QM/MM	−48.90	22.00	−51.28	19.49
	QM/MM/BP[a]	−49.33	21.95	−52.84	19.17

[a] Outer macromolecule region is represented by SMBP in geometry optimizations and by GSBP in FEP calculations.

region consisted of pOHB and the isoalloxazine part of FADHOOH up to the first methylene unit of the ribityl side chain that was saturated with a hydrogen link atom. The semiempirical AM1 Hamiltonian was employed to describe the QM part. The inner region was centered on the initial position of the distal oxygen atom of the hydroperoxo group of FADHOOH. All charge groups with any atom within 18.5 Å of the center belonged to the inner region and were modeled explicitly. All charge groups with any atom within 16 Å of the center belonged to the active region and were allowed to move.

In the hydroxylation step of the PHBH catalytic cycle, the OH unit of the hydroperoxo group of FADHOOH is transferred to the meta carbon atom of pOHB (see Figure 7). To compute the potential energy profile and split the reaction into discrete windows for the FEP calculations, a reaction coordinate was defined:

$$\zeta = d(O_d - O_p) - d(C_m - O_d) \qquad (28)$$

Here, O_d and O_p designate the distal and proximal oxygen atoms of the hydroperoxo unit of FADHOOH, respectively. C_m is the meta carbon atom of pOHB. Starting from the two initial structures, the stationary points of this reaction were located using the QM/MM and the QM/MM/SMBP Hamiltonian. Both methods yield similar results (Table 5). For configuration 1, QM/MM and QM/MM/SMBP geometry optimizations lead to slightly different local minima, as indicated by a root-mean-square (rms) deviation (of the active atoms) of 5.4 pm. However, the reaction and activation energies deviate by only 1.2 and 0.9 kcal/mol, respectively. These differences are in the same range as the differences between the two configurations on the pure QM/MM level. For configuration 2, both Hamiltonians lead to the same local minimum with a rms deviation of 0.8 pm. Hence, the reaction and activation energies differ by only 0.4 and 0.1 kcal/mol,
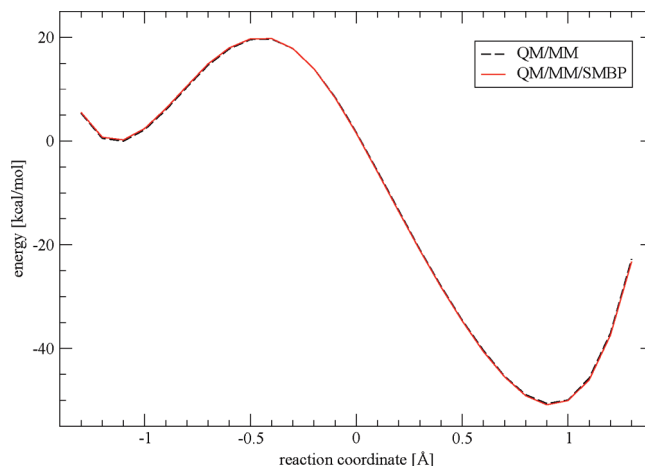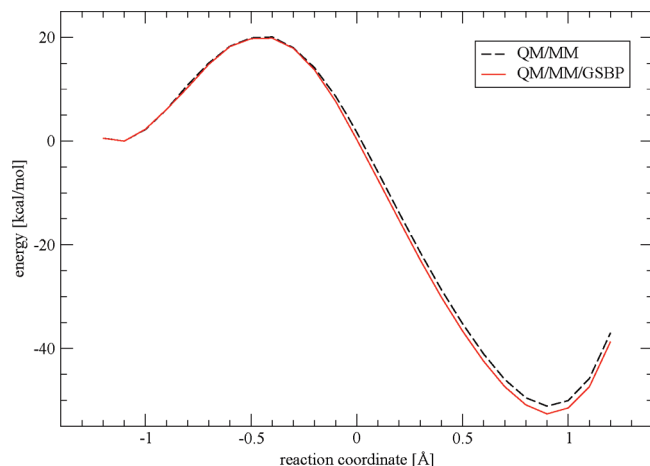

Figure 8. Potential energy profile of the OH transfer reaction in PHBH computed with QM/MM and QM/MM/SMBP independently (configuration 2). The QM atoms are described by the AM1 method and the MM atoms by the CHARMM force field.

respectively. The plot of the potential energy profile in Figure 8 illustrates this impressive agreement.

The optimized geometries of the discrete windows along the reaction coordinate were used as input structures to sample over the MM phase space in the framework of FEP. For each window, the QM atoms were fixed, and the QM charge density was approximated by constant ESP charges. For the structures that were optimized with the QM/MM/SMBP Hamiltonian, the GSBP could be applied to accelerate the MD steps. To avoid mobile water molecules or flexible residues approaching the boundary separating the inner and outer regions, the size of the active region was reduced in the QM/MM/GSBP calculations. Here, all atoms within 15 Å of the center were allowed to move. Moreover, a spherical restraint with a radius of 17 Å and a force constant of 0.004 au was applied to all active atoms to avoid any mobile residue leaving the inner region. For both Hamiltonians, the molecular structure in each window was equilibrated for 10 ps followed by a FEP production run of 10 ps. The resulting MD data was coarse-grained and subjected to a standard set of statistical tests to ensure a lack of trend and correlation.[10] If necessary, data points at the beginning of the production run were discarded (at most 4 ps so that production runs lasted at least 6 ps for each window).

For configuration 1, the free energies of activation and reaction deviate by 0.9 and 0.1 kcal/mol, respectively (Table 5). The results for configuration 2 are similar with deviations of 0.3 and 1.6 kcal/mol, respectively. Figure 9 illustrates that the free energy profiles computed with and without GSBP agree well for all stages of the reaction. In view of the other approximations that are necessary for QM/MM-FEP simulations, the deviations caused by the GSBP seem small and tolerable. Application of the GSBP offers massive computational savings. In the PHBH system, the computational time for a single MD step of the FEP calculation is reduced by 95% from 116.2 s to only 4.9 s (Table 6). Even when taking the GSBP overhead into account, the computational costs of QM/MM/GSBP-FEP calculations are roughly 1 order of magnitude smaller than those of standard QM/MM-FEP

Figure 9. Free energy profile of the OH transfer reaction in PHBH computed with QM/MM and QM/MM/GSBP independently (configuration 2, excluding entropic QM contributions). The QM atoms are described by the AM1 method and the MM atoms by the CHARMM force field.

Table 6. Computation Time per MD Step [s] in FEP Simulations of the PHBH Model System[a]

module	QM/MM	QM/MM/GSBP
MM energy+gradient	69.2	2.6
QM energy+gradient	0.4	0.0
FEP	46.6	2.2
GSBP		0.1
total	116.2	4.9

[a] All values are averaged over 200 MD steps and were computed serially on 2.6 GHz AMD Opteron machines with 16 GB of memory.

calculations. In modeling enzymatic reactions, the combination of SMBP and GSBP for geometry optimizations and FEP calculations thus offers good accuracy combined with high efficiency.

4.3. Cytochrome P450cam. A recent QM/MM study addressed the steric and electrostatic factors that affect the geometrical and electronic structure of the pentacoordinated cytochrome P450cam complexes.[88] Among other properties, the energies of the doublet and quartet states relative to the sextet state were found to be strongly influenced by the protein environment. Therefore, we have chosen the spin state energy gaps of the ferric complex as a challenging protein test system to see if the SMBP is able to reproduce such subtle energy differences.

The system setup was based on the X-ray structure of the ferric complex (PDB code 1DZ4)[99] that was subjected to a standard solvation and relaxation protocol, followed by a protonation procedure that led to a final system with a total charge of $-9e$. Our calculations started from the two structures selected previously from a classical MD simulation after 31 and 93 ps.[88] For the QM calculations, three different density functionals were used that combine Becke's B88 exchange functional[94] with a varying fraction of Hartree−Fock (HF) exchange and the Lee−Yang−Parr (LYP) correlation functional:[95] BLYP, B3LYP,[96] and BHLYP.[100] We used the 6-31+G* basis for all atoms coordinated to the iron and the 6-31G basis set for the remaining ligand atoms. The iron

atom was described by a Wachters all-electron basis set with additional sets of diffuse d and polarizing f functions.[101−103]

The QM region included the iron−porphyrin system of the heme unit and the sulfur atom of the coordinating Cys357 (with a hydrogen link atom attached to sulfur). The atoms of all residues with any atom within 4 Å of the heme−Cys357 complex or the camphor substrate were allowed to move; all other atoms were frozen. In the QM/MM/SMBP calculations, the inner region was centered on the initial position of the iron atom with an extended dielectric cavity radius of 29 Å. All residues with any atom within 20 Å of the iron atom belonged to the inner region and were described explicitly. The influence of all other residues was mimicked by the boundary potential.

The initial structures were first optimized in the sextet state with the QM/MM and the QM/MM/SMBP Hamiltonian, respectively. The two resulting geometries were subsequently reoptimized in the quartet and doublet state.

In the original study,[88] the B3LYP functional was found to provide the most realistic description of the spin state splittings with the correct sextet ground state, although the doublet−sextet gap is overestimated. Here, we are not interested in the absolute quality of the QM/MM results but want to know how well the QM/MM/SMBP approach can reproduce the QM/MM results. The values for the spin state energy gaps are given in Table 7. For eight out of 12 energy gaps, the QM/MM/SMBP results are within 0.1 kcal/mol of the full QM/MM results. The maximum absolute deviation is 0.21 kcal/mol, and the absolute deviations of the individual QM and MM components rarely exceed 0.4 kcal/mol. Moreover, subtle effects are reproduced very well: When the B3LYP functional is used, the QM calculation (in the field of the protein point charges) favors the quartet state over the sextet state by 0.71 kcal/mol in configuration 31. This preference is overcompensated by the MM contribution that favors the sextet state by 1.54 kcal/mol, leading to a QM/MM energy difference of 0.83 kcal/mol. In the QM/MM/SMBP calculations both components are reproduced almost exactly and sum up to an energy gap of 0.82 kcal/mol in favor of the sextet state. The results for configuration 93 are similar. These data show that the SMBP reproduces the electrostatic effects of the protein environment onto the QM and MM regions accurately, implying that geometry optimizations with the QM/MM/SMBP approach lead to highly similar local minima on the potential energy surface compared to standard QM/MM optimizations. This is corroborated by a direct comparison of the QM/MM and QM/MM/SMBP optimized geometries in Table S5 (Supporting Information): The rms deviations (of the active atoms) are usually around 1 pm or less. Only for the B3LYP optimized structures of configuration 31 are there larger rms deviations of about 6 pm. These can be traced back to a 30° rotation of a methyl group attached to the porphine ring in a hydrophobic environment. However, the corresponding spin state gaps are not affected by this peripheral conformational change and match almost perfectly.

In summary, optimizations with the QM/MM/SMBP Hamiltonian lead to biomolecular structures that either are almost identical to those from full QM/MM optimizations or they represent nearby local minima which are as representative for the molecular and electronic structure of the

Table 7. Sextet−Quartet and Sextet−Doublet Energy Gaps in Cytochrome P450cam [in kcal/mol] Computed with the Standard QM/MM and the Approximated QM/MM/SMBP Hamiltonian for Two Configurations and Three Different Density Functionals (BLYP, B3LYP, BHLYP)

snapshot	Hamiltonian	gap	BLYP QM/MM	QM	MM	B3LYP QM/MM	QM	MM	BHLYP QM/MM	QM	MM
31	QM/MM	$E(^4A)-E(^6A)$	−9.50	−11.31	1.81	0.83	−0.71	1.54	16.49	14.40	2.09
		$E(^2A)-E(^6A)$	−9.98	−9.74	−0.24	6.94	7.11	−0.18	28.80	28.92	−0.12
	QM/MM/SMBP	$E(^4A)-E(^6A)$	−9.63	−10.89	1.26	0.82	−0.74	1.56	16.50	14.42	2.08
		$E(^2A)-E(^6A)$	−10.19	−9.80	−0.39	7.10	7.00	0.10	28.70	28.34	0.36
93	QM/MM	$E(^4A)-E(^6A)$	−9.52	−11.00	1.48	0.73	−0.98	1.72	16.40	13.69	2.72
		$E(^2A)-E(^6A)$	−10.66	−10.49	−0.17	6.33	6.75	−0.43	28.74	28.96	−0.22
	QM/MM/SMBP	$E(^4A)-E(^6A)$	−9.54	−10.62	1.08	0.83	−0.83	1.67	16.34	13.69	2.65
		$E(^2A)-E(^6A)$	−10.70	−10.32	−0.39	6.44	6.36	0.08	28.66	29.00	−0.35

biomolecule as those resulting from standard QM/MM optimizations.

5. Conclusion

In this article, we have introduced a general boundary potential (SMBP) for hybrid QM/MM calculations that complements the previously implemented boundary potential (GSBP). Both the SMBP and the GSBP extend the QM/MM approach to a three-layer model in which the outer solvent molecules and outer macromolecule region are represented by a boundary potential. Therefore, both account for the effect of bulk solvent and treat long-range electrostatic interactions accurately and efficiently. In both cases, the reaction field potential in the inner region needs to be computed by a finite-difference solution of the Poisson−Boltzmann equation (describing the bulk solvent as a dielectric continuum). In the GSBP scheme, this inner reaction field potential is expressed by its Green's function and is represented by a reaction field matrix that is determined once and for all at the beginning of a simulation and is then used to calculate the corresponding electrostatic interactions with the inner region charge density. In the SMBP scheme, the inner reaction field potential is computed on-the-fly as needed, and the interactions with the QM density are handled by a self-consistent reaction field procedure and a set of virtual surface charges that represent the SMBP in the QM calculations.

The GSBP performs best in MD simulations where the initial overhead for constructing the reaction field matrix (typically about 800 Poisson−Boltzmann calculations) is quickly overcompensated by the gains in each of the many steps during the MD simulation. The SMBP targets single-point calculations and geometry optimizations with a limited number of steps where the on-the-fly approach is most efficient. Since the approximations in the GSBP and SMBP treatments are very similar by design, and compatible with each other, the electronic and molecular structures resulting from QM/MM/SMBP geometry optimizations can be used as starting points for sampling over MM phase space using the QM/MM/GSBP Hamiltonian in the FEP framework. Free energy calculations on the PHBH enzyme show that this reduces the computational costs of the FEP calculations by 1 order of magnitude. The combined use of the SMBP and GSBP for computing potential energy profiles and subsequent sampling, respectively, thus provides an attractive and efficient strategy to perform free energy QM/MM calculations.

The GSBP implementation at the QM/MM level requires modifications of the underlying QM code, and corresponding work has been reported up to now only for semiempirical QM methods.[20,21] By contrast, because of its representation in terms of virtual surface charges, the SMBP can be used with any standard QM code that can handle external point charges, thus allowing for ab initio QM/MM/SMBP and DFT/MM/SMBP geometry optimizations in the context of three-layer QM/MM/continuum models. Another practical advantage of the SMBP is that it also offers significant speedups for standard two-layer QM/MM calculations: thousands of MM charges are replaced by a small set of virtual surface charges (with little overhead since no SCRF procedure is required in this case) whose electrostatic interactions with the inner region are easily computed (with overall savings typically by a factor of 2).

The accuracy of the SMBP has been evaluated by comparing the results from QM/MM/SMBP calculations to those from standard QM/MM calculations for three diverse test systems: Glycine in water turned out to be problematic for the SMBP. Due to the high flexibility of the polar solvent, many close-lying minima with different hydrogen-bond patterns and different relative energies exist, and as a consequence, geometry optimizations by QM/MM and QM/MM/SMBP normally follow a different course and yield different local minima (unless starting from a given QM/MM minimum which is retained by QM/MM/SMBP). The individual reaction and activation energies for proton transfer in solvated glycine thus differ appreciably between QM/MM and QM/MM/SMBP, while the mean values for a small sample of five configurations are much closer to each other (within 1 kcal/mol). The two enzymatic test systems are more rigid. They are treated by the SMBP with impressive accuracy. Geometry optimizations by QM/MM and QM/MM/SMBP normally follow the same course and lead to essentially identical structures, and relative energies differ on average by less than 1 kcal/mol. The magnitude of these deviations is comparable to the spread of results that naturally occurs for different initial configurations. Finally, in the case of PHBH, the combined use of the SMBP and GSBP leads to free energy profiles and barriers that are essentially the same as those from full QM/MM calculations. We conclude that these boundary potentials enable us to treat enzymes at the QM/MM level efficiently and with good accuracy.

Note Added after ASAP Publication. This article was published ASAP on October 14, 2009. Table 3 has been modified. The correct version was published on October 22, 2009.

Supporting Information Available: Details of the glycine/water test system; evaluation of the accuracy of the electrostatic forces for the glycine/water system in bulk solvent and in vacuum; rms deviations of the QM/MM and QM/MM/SMBP optimized structures of cytochrome P450cam. This information is available free of charge via the Internet at http://pubs.acs.org.

References

(1) Hu, H.; Yang, W. *Annu. Rev. Phys. Chem.* **2008**, *59*, 573–601.

(2) Zhang, Y.; Liu, H.; Yang, W. *J. Chem. Phys.* **2000**, *112*, 3483–3492.

(3) Cisneros, G. A.; Liu, H.; Zhang, Y.; Yang, W. *J. Am. Chem. Soc.* **2003**, *125*, 10384–10393.

(4) Ridder, L.; Rietjens, I. M. C. M.; Vervoort, J.; Mulholland, A. J. *J. Am. Chem. Soc.* **2002**, *124*, 9926–9936.

(5) Kaminski, G. A.; Jorgensen, W. L. *J. Phys. Chem. B* **1998**, *102*, 1787–1796.

(6) Acevedo, O.; Jorgensen, W. L.; Evanseck, J. D. *J. Chem. Theory Comput.* **2007**, *3*, 132–138.

(7) Rod, T. H.; Ryde, U. *J. Chem. Theory Comput.* **2005**, *1*, 1240–1251.

(8) Strajbl, M.; Hong, G.; Warshel, A. *J. Phys. Chem. B* **2002**, *106*, 13333–13343.

(9) Senn, H. M.; Thiel, S.; Thiel, W. *J. Chem. Theory Comput.* **2005**, *1*, 494–505.

(10) Kästner, J.; Senn, H. M.; Thiel, S.; Otte, N.; Thiel, W. *J. Chem. Theory Comput.* **2006**, *2*, 452–461.

(11) Senn, H. M.; Thiel, W. *Top. Curr. Chem.* **2007**, *268*, 173–290.

(12) Senn, H. M.; Thiel, W. *Angew. Chem., Int. Ed.* **2009**, *48*, 1198–1229.

(13) Warshel, A.; Papazyan, A. *Curr. Opin. Struct. Biol.* **1998**, *2*, 211–217.

(14) Sagui, C.; Darden, T. A. *Annu. Rev. Biophys. Struct.* **1999**, *28*, 155–179.

(15) Davis, M. E.; McCammon, J. A. *Chem. Rev.* **1990**, *90*, 509–521.

(16) Garcia-Viloca, M.; Gao, J.; Karplus, M.; Truhlar, D. G. *Science* **2004**, *303*, 186–195.

(17) Nam, K.; Gao, J.; York, D. M. *J. Chem. Theory Comput.* **2005**, *1*, 2–13.

(18) Gao, J.; Alhambra, C. *J. Chem. Phys.* **1997**, *107*, 1212–1217.

(19) Walker, R. C.; Crowley, M. F.; Case, D. A. *J. Comput. Chem.* **2008**, *29*, 1019–1031.

(20) Schaefer, P.; Riccardi, D.; Cui, Q. *J. Chem. Phys.* **2005**, *123*, 014905/1−14.

(21) Benighaus, T.; Thiel, W. *J. Chem. Theory Comp.* **2008**, *4*, 1600–1609.

(22) Friedman, H. L. *Mol. Phys.* **1975**, *29*, 1533–1543.

(23) Wang, L.; Hermans, J. *J. Phys. Chem.* **1995**, *99*, 12001–12007.

(24) Berkowitz, M.; McCammon, J. A. *Chem. Phys. Lett.* **1982**, *90*, 215–217.

(25) Brooks, III, C. L.; Karplus, M. *J. Chem. Phys.* **1983**, *79*, 6312–6325.

(26) Brunger, A.; Brooks, III, C. L.; Karplus, M. *Chem. Phys. Lett.* **1984**, *105*, 495–500.

(27) Brunger, A.; Brooks, III, C. L.; Karplus, M. *Proc. Natl. Acad. Sci. U.S.A.* **1985**, *82*, 8458–8462.

(28) Lee, F. S.; Warshel, A. *J. Chem. Phys.* **1992**, *97*, 3100–3107.

(29) Alper, H.; Levy, R. M. *J. Chem. Phys.* **1993**, *99*, 9847–9852.

(30) Essex, J. W.; Jorgensen, W. L. *J. Comput. Chem.* **1995**, *16*, 951–972.

(31) Warshel, A.; King, G. *Chem. Phys. Lett.* **1985**, *121*, 124–129.

(32) Tironi, I. G.; Sperb, R.; Smith, P. E.; van Gunsteren, W. F. *J. Chem. Phys.* **1995**, *102*, 5451–5459.

(33) Beglov, D.; Roux, B. *J. Chem. Phys.* **1994**, *100*, 9050–9063.

(34) Im, W.; Bernèche, S.; Roux, B. *J. Chem. Phys.* **2001**, *114*, 2924–2937.

(35) Banavali, N. K.; Im, W.; Roux, B. *J. Chem. Phys.* **2002**, *117*, 7381–7388.

(36) Elstner, M.; Porezag, D.; Jungnickel, G.; Elstner, J.; Haugk, M.; Frauenheim, T.; Suhai, T.; Seifert, G. *Phys. Rev. B* **1998**, *58*, 7260–7268.

(37) König, P. H.; Ghosh, N.; Hoffmann, M.; Elstner, M.; Tajkhorshid, E.; Frauenheim, T.; Cui, Q. *J. Phys. Chem. A* **2006**, *110*, 548–563.

(38) Ma, L.; Cui, Q. *J. Am. Chem. Soc.* **2007**, *129*, 10261–10268.

(39) Zhu, X.; Jethiray, A.; Cui, Q. *J. Chem. Theory Comput.* **2007**, *3*, 1538–1549.

(40) Riccardi, D.; König, P.; Prat-Resina, X.; Yu, H.; Elstner, M.; Frauenheim, T.; Cui, Q. *J. Am. Chem. Soc.* **2006**, *128*, 16302–16311.

(41) Riccardi, D.; Schaefer, P.; Cui, Q. *J. Phys. Chem. B* **2005**, *109*, 17715–17733.

(42) Chandrasekhar, J.; Smith, S. F.; Jorgensen, W. L. *J. Am. Chem. Soc.* **1984**, *106*, 3049–3059.

(43) Chandrasekhar, J.; Jorgensen, W. L. *J. Am. Chem. Soc.* **1985**, *107*, 2974–2975.

(44) Jorgensen, W. L. *Acc. Chem. Res.* **1989**, *22*, 184–189.

(45) Chandrasekhar, J.; Smith, S. F.; Jorgensen, W. L. *J. Am. Chem. Soc.* **1985**, *107*, 154–163.

(46) Kuhn, B.; Kollmann, P. A. *J. Am. Chem. Soc.* **2000**, *122*, 2586–2596.

(47) Kollmann, P. A.; Kuhn, B.; Donini, O.; Perakyla, M.; Stanton, R.; Bakowies, D. *Acc. Chem. Res.* **2001**, *34*, 72–79.

(48) Bentzien, J.; Mueller, R. P.; Floriá, J.; Warshel, A. *J. Phys. Chem. B* **1998**, *102*, 2293–2301.

(49) Olsson, M. H. M.; Hong, G.; Warshel, A. *J. Am. Chem. Soc.* **2003**, *125*, 5025–5039.

(50) Warshel, A. *Annu. Rev. Biophys. Biomol. Struct.* **2003**, *32*, 425–443.

(51) Zwanzig, R. W. *J. Chem. Phys.* **1954**, *22*, 1420–1426.

(52) Cisneros, G. A.; Wang, M.; Silinski, P.; Fitzgerald, M. C.; Yang, W. *Biochemistry* **2004**, *43*, 6885–6892.

(53) Wang, M.; Lu, Z.; Yang, W. *J. Chem. Phys.* **2004**, *121*, 101–107.

(54) Donini, O.; Darden, T.; Kollman, P. A. *J. Am. Chem. Soc.* **2000**, *122*, 12270–12280.

(55) Klapper, I.; Hagstrom, R.; Fine, R.; Sharp, K.; Honig, B. *Proteins* **1986**, *1*, 47–59.

(56) Sherwood, P.; et al. *J. Mol. Struct. (THEOCHEM)* **2003**, *632*, 1–28.

(57) Mulliken, R. S. *J. Chem. Phys.* **1962**, *36*, 3428–3439.

(58) Tannor, D. J.; Marten, B.; Murphy, R.; Friesner, R. A.; Sitkoff, D.; Nicholls, A.; Honig, B.; Ringnalda, M.; Goddard, W. A. *J. Am. Chem. Soc.* **1994**, *116*, 11875–11882.

(59) Hayik, S. A.; Liao, N.; Merz, K. M. *J. Chem. Theory Comput.* **2008**, *4*, 1200–1207.

(60) Im, W.; Beglov, D.; Roux, B. *Comput. Phys. Commun.* **1998**, *111*, 59–75.

(61) Bakowies, D.; Thiel, W. *J. Phys. Chem.* **1996**, *100*, 10580–10594.

(62) Jensen, F. Transition State Theory and Statistical Mechanics. In *Introduction to Computational Chemistry;* John Wiley & Sons: Chichester; England, **1999**; pp 301–304.

(63) ChemShell. http://www.chemshell.org (accessed August 14, 2009).

(64) Thiel, W. MNDO2004; Max-Planck-Institut für Kohlenforschung: Mülheim an der Ruhr, Germany, 2004.

(65) Ahlrichs, R.; Bär, M.; Häser, M.; Horn, H.; Kölmel, C. *Chem. Phys. Lett.* **1989**, *162*, 165–169.

(66) Smith, W.; Forester, T. *J. Mol. Graph.* **1996**, *14*, 136–141.

(67) MacKerell, A. D.; et al. *J. Phys. Chem. B* **1998**, *102*, 3586–3616.

(68) Billeter, S. R.; Turner, A. J.; Thiel, W. *Phys. Chem. Chem. Phys.* **2000**, *2*, 2177–2186.

(69) Press, W. H.; Flannery, B. P.; Teukolsky, S. A.; Vetterlig, W. T. Partial Differential Equations. In *Numerical Recipes in C*; Cambridge University Press: Cambridge, England, 1988; pp 673−680.

(70) Nicholls, A.; Honig, B. *J. Comput. Chem.* **1991**, *12*, 435–445.

(71) Im, W.; Seefeld, S.; Roux, B. *Biophys. J.* **2000**, *79*, 788–801.

(72) Nosé, S. *J. Chem. Phys.* **1984**, *81*, 511–519.

(73) Nosé, S. *Mol. Phys.* **1984**, *52*, 255–268.

(74) Hoover, W. G. *Phys. Rev. A* **1985**, *31*, 1695–1697.

(75) Martyna, G. J.; Klein, M. L.; Tuckerman, M. *J. Chem. Phys.* **1992**, *97*, 2635–2643.

(76) Ryckaert, J.-P.; Ciccotti, G.; Berendsen, H. J. C. *J. Comput. Phys.* **1977**, *23*, 327–341.

(77) Bandyopadhyay, P.; Gordon, M. S. *J. Chem. Phys.* **2000**, *113*, 1104–1109.

(78) Bandyopadhyay, P.; Gordon, M. S.; Mennucci, B.; Tomasi, J. *J. Chem. Phys.* **2002**, *116*, 5023–5032.

(79) Gontrani, L.; Mennucci, B.; Tomasi, J. *J. Mol. Struct. (THEOCHEM)* **2000**, *500*, 113–127.

(80) Cui, Q. *J. Chem. Phys.* **2002**, *117*, 4720–4728.

(81) Claeyssens, F.; Harvey, J. N.; Manby, F. R.; Mata, R. A.; Mulholland, A. J.; Ranaghan, K. E.; Schütz, M.; Thiel, S.; Thiel, W.; Werner, H.-J. *Angew. Chem., Int. Ed.* **2006**, *45*, 6856–6859.

(82) Mata, R. A.; Werner, H.-J.; Thiel, S.; Thiel, W. *J. Chem. Phys.* **2008**, *128*, 025104/1−8.

(83) Ridder, L.; Mulholland, A. J.; Vervoort, J.; Rietjens, I. M. C. M. *J. Am. Chem. Soc.* **1998**, *120*, 7641–7642.

(84) Ridder, L.; Harvey, J. N.; Rietjens, I. M. C. M.; Vervoort, J.; Mulholland, A. J. *J. Phys. Chem. B* **2003**, *107*, 2118–2126.

(85) Billeter, S. R.; Hanser, C. F. W.; Mordasini, T. Z.; Scholten, M.; Thiel, W.; van Gunsteren, W. F. *Phys. Chem. Chem. Phys.* **2001**, *3*, 688–695.

(86) Shaik, S.; Kumar, D.; de Visser, S. P.; Altun, A.; Thiel, W. *Chem. Rev.* **2005**, *105*, 2279–2328.

(87) Shaik, S.; Cohen, S.; Wang, Y.; Chen, H.; Kumar, D.; Thiel, W. *Chem. Rev.* ASAP article, DOI: 10.1021/cr900121s.

(88) Altun, A.; Thiel, W. *J. Phys. Chem. B* **2005**, *109*, 1268–1280.

(89) Woo, H.-J.; Dinner, A. R.; Roux, B. *J. Chem. Phys.* **2004**, *121*, 6392–6400.

(90) Deng, Y.; Roux, B. *J. Chem. Phys.* **2008**, *128*, 115103/1−8.

(91) Brooks, B. R.; Bruccoleri, R. E.; Olafson, B. D.; States, D. J.; Swaminathan, S.; Karplus, M. *J. Comput. Chem.* **1983**, *4*, 187–217.

(92) Dewar, M. J. S.; Zoebisch, E. G.; Healy, E. F.; Stewart, J. J. P. *J. Am. Chem. Soc.* **1985**, *107*, 3902–3909.

(93) Gilson, M. K.; Sharp, K. A.; Honig, B. H. *J. Comput. Chem.* **1987**, *9*, 327–335.

(94) Becke, A. D. *Phys. Rev. A* **1988**, *38*, 3098–3100.

(95) Lee, C.; Yang, W.; Parr, R. G. *Phys. Rev. B* **1988**, *37*, 785–789.

(96) Becke, A. D. *J. Chem. Phys.* **1993**, *98*, 5648–5652.

(97) Schäfer, A.; Horn, H.; Ahlrichs, R. *J. Chem. Phys.* **1992**, *97*, 2571–2577.

(98) Schäfer, A.; Huber, C.; Ahlrichs, R. *J. Chem. Phys.* **1994**, *100*, 5829–5835.

(99) Schlichting, I.; Berendzen, J.; Chu, K.; Stock, A. M.; Maves, S. A.; Benson, D. E.; Sweet, R. M.; Ringe, D.; Petsko, G. A.; Sligar, S. G. *Science* **2000**, *287*, 1615–1622.

(100) Becke, A. D. *J. Chem. Phys.* **1993**, *98*, 1372–1377.

(101) Wachters, A. J. H. *J. Chem. Phys.* **1970**, *52*, 1033–1036.

(102) Hay, P. J. *J. Chem. Phys.* **1977**, *66*, 4377–4384.

(103) Bauschlicher, C. W., Jr.; Langhoff, S. R.; Partridge, H.; Barnes, L. A. *J. Chem. Phys.* **1989**, *91*, 2399–2411.